Integration of a gas pressure chamber on a reciprocal tribometer for experiments at ambient pressures up to 10 bar

Florian Ausserer
Research Unit Tribology, Institute of Engineering Design and Product Development, TU Wien, Wien, Austria
Igor Velkavrh
Department of Tribo Design, V-Research, Dornbirn, Austria
Fevzi Kafexhiu
Department of Tribo Design, V-Research GmbH, Dornbirn, Austria, and
Carsten Gachot
Research Unit Tribology, Institute of Engineering Design and Product Development, TU Wien, Wien, Austria

Abstract

Purpose – This study aims to focus on the development of an experimental setup for testing tribological pairings under a gas atmosphere at pressures up to 10 bar.

Design/methodology/approach – A pressure chamber allowing oscillating movement through an outer shaft was constructed and mounted on an oscillating tribometer. Due to a metal spring bellows system, a methodology for the evaluation of the coefficient of friction values separately from the spring forces was developed.

Findings – The selected material concept was qualitatively and quantitatively assessed. An evaluation of the static and the dynamic coefficient of friction was performed, which was crucial for the understanding of the adhesion effects of the tested material pairing. The amount of information that is lost due to averaging the measured friction values is higher than one would expect.

Originality/value – The developed experimental setup is unique and, compared with the existing tribometers for testing under gas ambient pressures, allows testing under contact conditions that are closer to real applications, such as compressors and expanders. An in-depth observation of the adhesion and stick–slip effects of the tested material pairings is possible as well.

Peer review – The peer review history for this article is available at: https://publons.com/publon/10.1108/ILT-06-2023-0173/

Keywords Friction, Wear, Tribometer, Gas pressure chamber, Sealings

Paper type Research paper

1. Introduction

It is known from various studies that the atmospheric environment of a tribological contact significantly affects its frictional and wear behaviour. The influence of the oxygen (O_2) atmosphere on the sliding friction of pure iron was investigated by Buckley (1981). In the absence of oxides, under an ultra-high vacuum of 10^{-10} Torr, a high coefficient of friction of around 4 was measured. With the gradual addition of oxygen, iron oxides (FeO, Fe_3O_4 and Fe_2O_3) were formed, decreasing the metal–metal adhesion and thus significantly reducing the coefficient of friction. In another study (Mishina, 1995), it was reported that in an O_2 atmosphere in high-speed pin-on-disk contacts, a thin oxide layer formed on chromium steel, which reduced the wear rate as compared to nitrogen (N_2), i.e. an oxygen-free atmosphere. In addition, compared to O_2 and carbon dioxide (CO_2) atmospheres, a higher adhesion tendency was reported in an N_2 atmosphere. Furthermore, it was already shown by the authors (Velkavrh *et al.*, 2016) that in the CO_2 atmosphere, significantly lower friction and wear values of 100Cr6 steel/steel contacts were measured than in air, Ar and N_2

The current issue and full text archive of this journal is available on Emerald Insight at: **https://www.emerald.com/insight/0036-8792.htm**

Industrial Lubrication and Tribology
75/8 (2023) 911–918
Emerald Publishing Limited [ISSN 0036-8792]
[DOI 10.1108/ILT-06-2023-0173]

Special thanks to the AWS – promotional bank of the Austrian federal government – for funding this work as part of the Preseed program (Project Nr. P1910189-PSI01). Parts of the work presented were also funded by the Austrian COMET Program (Project InTribology, no. 872176) and carried out at the "Excellence Centre of Tribology" (AC2T research GmbH) in collaboration with V-Research GmbH and fautech gmbH. Funding by the Austrian Cooperative Research (Project SlipIT, no. SP-2021-05) is gratefully acknowledged.

Received 14 June 2023
Revised 21 July 2023
Accepted 24 July 2023

atmospheres. In CO_2, tribofilms consisting of iron carbonate $FeCO_3$ and/or iron bicarbonate $Fe_2(CO_3)_3$ were detected, which may be responsible for providing the low friction and low wear behaviour in this atmosphere.

In addition to metallic contacts, polymers also represent an important group of materials in gas tribology, especially in the sealing of moving or stationary components. Additional requirements in mechanical engineering and new trends, such as the use of CO_2 as a cooling medium (Ma *et al.*, 2013) or hydrogen (H_2) as a fuel (Teoh *et al.*, 2023), require the development and adjustment of polymers for these systems. In addition, there is a trend to reduce or eliminate the use of lubricants, as oil-free operation usually results in reduced investment and maintenance costs and improved heat exchange conditions (Kus and Nekså, 2013).

Although some tribological studies using polymers in CO_2 atmosphere can be found in the literature (Demas and Polycarpou, 2008; Nunez *et al.*, 2010; Yeo and Polycarpou, 2012), there is a lack of understanding about their behaviour. CO_2 can diffuse into polymers faster than into metals and can cause changes in polymer density (Eggers, 2005), as well as their chemical structure and thus affect their friction and wear behaviour (Dascalescu *et al.*, 2009). Furthermore, in the range of low and moderate loads, polymer friction decreases with decreasing load, which can lead to increased static friction and stick–slip effects (Myshkin *et al.*, 2005). Thus, for an optimal design of lubricant-free gas tribological systems, it is essential to characterize the tribological properties of these materials under realistic operating conditions, i.e. under a pressurized gas atmosphere and by considering the transitions between the static and the sliding friction.

Very few tribometers exist that allow investigations of gas tribological phenomena with pressure application, and in oscillatory movement execution, which enable periodic transitions between static and sliding friction. Furthermore, there are no scientific contributions that outline a methodology required to measure under these conditions. In the present study, a new measuring system was developed with which gas tribological experiments can be carried out at normal forces of 1 to 1,000 N and up to 10 bar overpressures. The experimental setup, methodology and example measurements are presented.

2. Methodology

2.1 Implementation and setup of the gas pressure module

A modular friction and wear test rig (RVM1000, Werner Stehr Tribologie GmbH, Germany) was modified with a gas pressure module (Figure 1), which allowed for testing under a gas atmosphere. The tribometer is powered by a rotational drive that can reach a maximum speed of 3,000 rpm. To convert this rotational movement into linear-oscillating motion, push–pull rods are used. The current setup allows for a maximum stroke of 6 mm. The pressure module, indicated by a blue dotted line in Figure 1, is attached to the load cell and can withstand gas pressures of up to 10 bar and temperatures of up to 100°C. The gas pressure is measured by a digital manometer, the reaction forces are measured by the load cell and the wear by a digital dial gauge. To apply the normal force, a pneumatic ram is used, which can exert a maximum force of 1,000 N.

Figure 1 Modular friction and wear test rig (RVM1000) with a pressure module, indicated by a blue dotted line

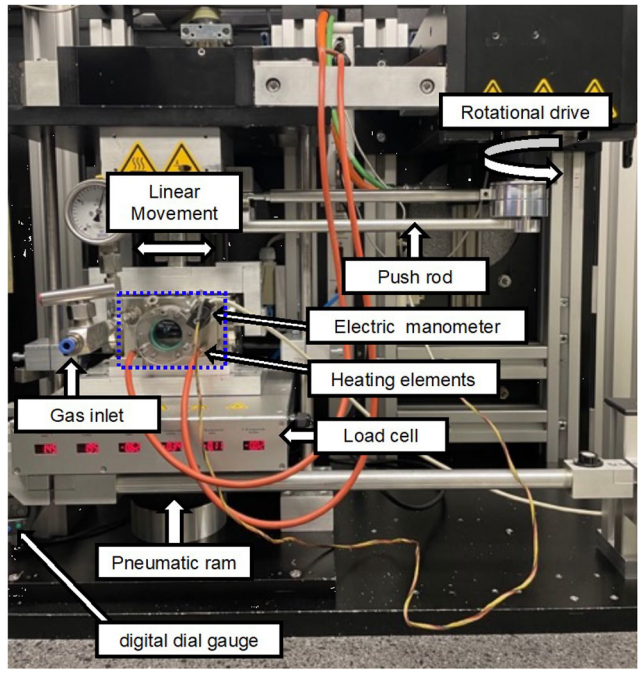

Source: Created by authors

Figure 2 provides a cross-sectional model of the gas pressure chamber. The upper sample is specifically designed to ensure surface contact with a self-aligning polymer sample, as shown in Figure 2(a). To ensure a tight seal, metal spring bellows (MSBs) are used in the gas pressure chamber. These bellows are attached to both the gas pressure chamber and the sample holder and have been engineered to accommodate a displacement of up to ±3 mm without exceeding the fatigue strength range of the MSBs. In Figure 2(b), a simple force path (red) is illustrated. The sample holder is constructed as a rigid body, which results in the upper sample experiencing a displacement force due to the conservation of force when the sample holder is moved linearly. The forces that arise during this process are measured with a load cell, and the measured displacement force is a sum of the MSB forces and the displacement force.

2.2 Evaluation of the coefficient of friction

Figure 3 illustrates the mechanical equivalent diagrams of the gas pressure module, where a rotational movement is converted into a linear movement resulting in a half-sine cycle from $-x$ to $+x$. The load cell measures the occurring forces on the left and the right, FM_l and FM_r. The zero-position $x_{(dp)} = 0$ is marked with a dashed-dotted line, and the lower specimen is rigid while the upper specimen is displaced relative to it.

To determine the actual friction value, it is important to subtract the MSB forces from the measured displacement force ($\vec{F}_{dp}$). In Figure 3(a), when the upper specimen is at position ($-x$), a displacement force ($\vec{F}_{dp}$) is required to move it to the $+x$ position. Due to the compression of MSB-left, a force $\vec{F}_{MSB\_l}$ acts in the direction of $\vec{F}_{dp}$, while the tensioned MSB-

Figure 2 Cross-sectional model of the gas pressure chamber

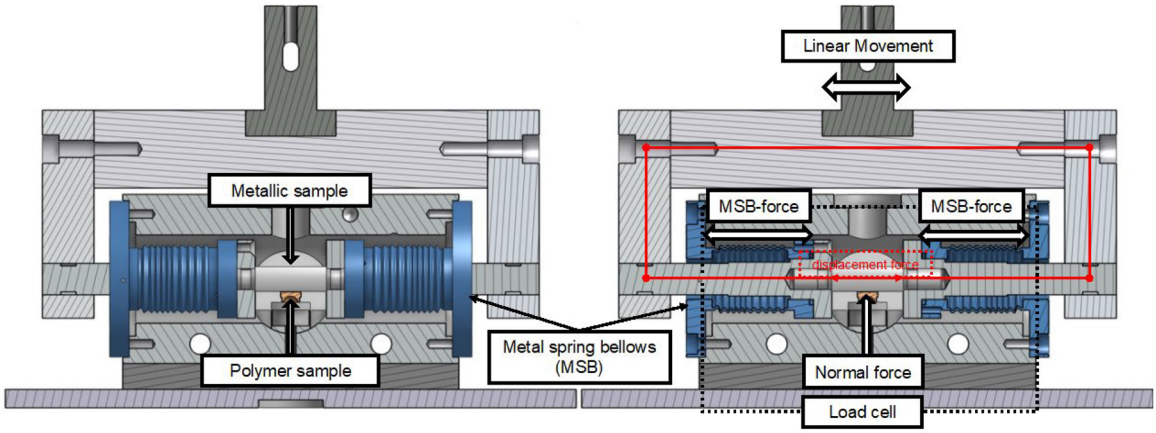

Source: Created by author

Figure 3 Mechanical equivalent diagrams representing the distribution of forces during the oscillating movement of the upper sample together with the deformation of the metal spring bellows

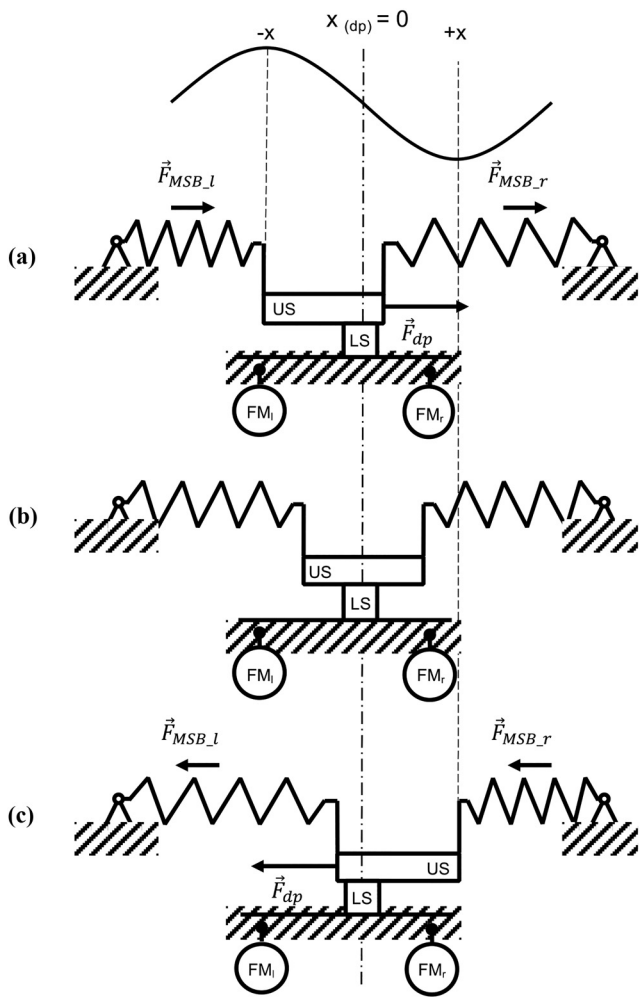

Source: Created by authors

right results in $\vec{F}_{MSB\_r}$ acting in the same direction. Figure 3(b) shows the neutral position of the upper sample where the sum of all forces is zero. In Figure 3(c), when the upper specimen is at the $+x$ position, a displacement force $(-\vec{F}_{dp})$ is necessary to move it to the $-x$ position. The compression of MSB-right results in $\vec{F}_{MSB\_r}$ acting in the direction of $-\vec{F}_{dp}$, while the tensioned MSB-left leads to $\vec{F}_{MSB\_l}$ acting in the same direction.

The evaluation electronics of the RVM calculates F_{dp} from the measured values of FM_l and FM_r as:

$$F_{dp} = FM_l + FM_r \tag{1}$$

However, to obtain $F_{dp-corr}$, which is the corrected value of F_{dp}, it is necessary to subtract F_{MSB_l} and F_{MSB_r} from F_{dp} at each point in time.

Therefore, the equation for:

$$F_{dp-corr} = (FM_l - F_{MSB\_l}) + (FM_r - F_{MSB_r}) \tag{2}$$

as demonstrated in the discussed cases.

For the calculation of the COF, the $F_{dp-corr}$ is divided by the normal force:

$$COF = \frac{F_{dp-corr}}{F_N} \tag{3}$$

2.3 Signal analysis of tribometer raw data

As mentioned in the previous section, to obtain the displacement (friction) force value ($F_{dp-corr}$), it is necessary to subtract the left and right force values from the measurement (a sum of both displacement and spring bellows forces) with the respective left and right forces from the calibration (characterized by spring bellows forces only) at each point in time.

In the current scenario, the data is sampled at a rate of 1 kHz, resulting in 1,000 points per second. Before subtracting the signals, it is essential to synchronize the measurement and calibration signals because they represent two distinct measurements. The purpose of synchronization is to account for the phase difference between the measurement and

Figure 4 An example out-of-phase signal is presented in (a) and (b), which represent measurement signals (FM_l and FM_r) and calibration signals (F_{MSB_l} and F_{MSB_r}) along with the selected synchronization points. (c) and (d) demonstrate the synchronized signals by applying time-wise shifting to the calibration data

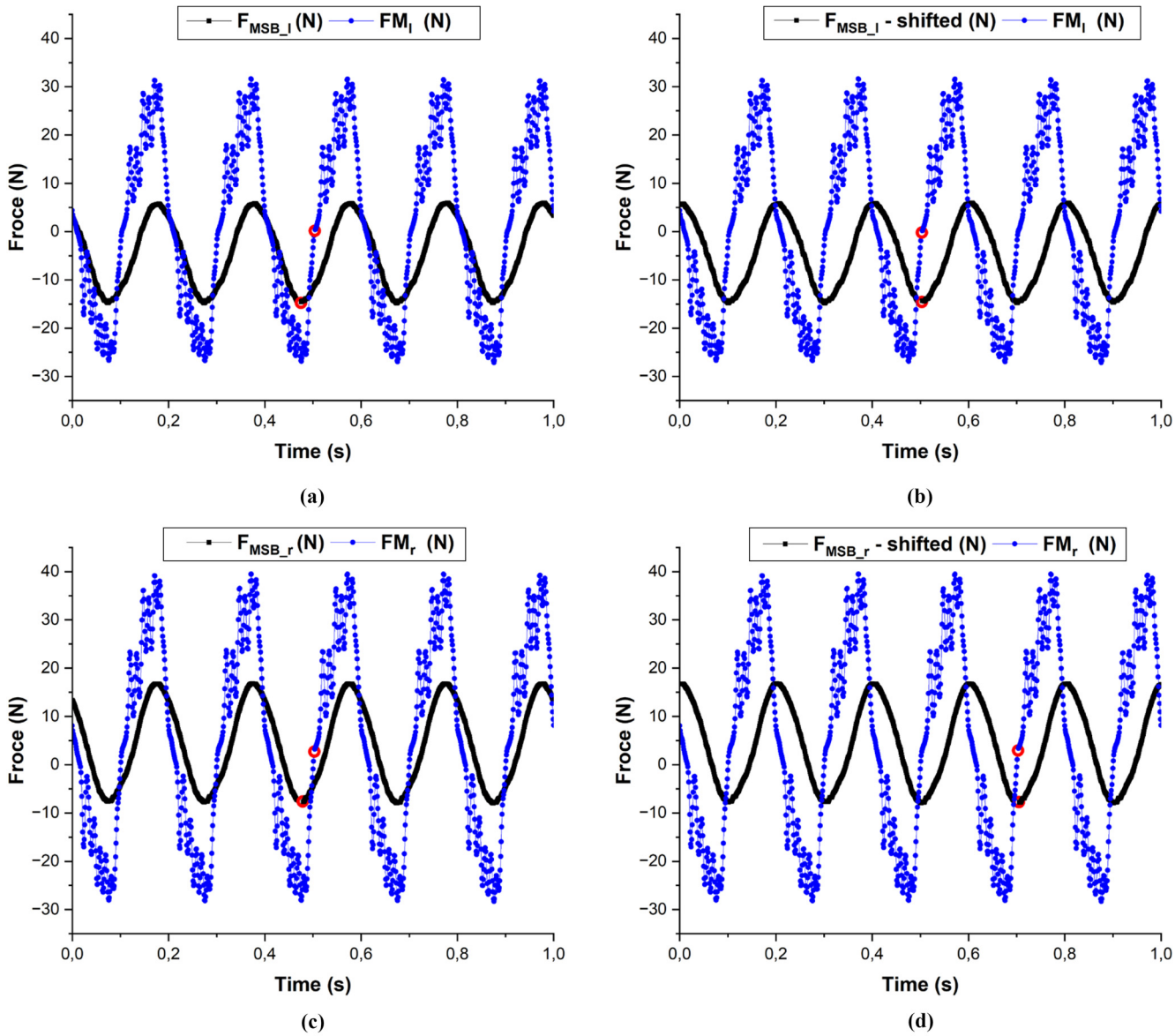

Source: Created by authors

calibration signals. This phase difference arises due to the practical impossibility of initiating two separate measurements from precisely the same starting position of the upper sample relative to the lower sample.

The synchronization process is designed to locate the minimum values in the calibration signals F_{MSB_l} and F_{MSB_r} shown in Figure 4(a) and 4(b) that are temporally closest to the average point, zero-crossing of the y-axis, between the minimum and maximum values of the measurement signals FM_l and FM_r. The calibration signals are adjusted in time to ensure that the synchronization points (represented by red circles) align with the corresponding points in the measurement signals, as depicted in Figure 4(c) and 4(d). At these synchronized points, the MSB force (F_{MSB}) reaches its peak, and the direction of the reciprocal motion is reversed, either from left to right or vice versa.

However, upon examining the entire time range of both signals (0–60 s), it becomes apparent that despite the synchronization, a progressive phase shift occurs over time. This phase shift is illustrated in Figure 5. The shift was quantified by determining the time difference between the minimum values of the calibration signals and the average values of the measurement signals within each cycle (stroke).

In addition to the increasing phase shift, both the calibration and measurement signals exhibit slight fluctuations, leading to

Figure 5 Quantified time difference (shift) between the calibration and measurement signals

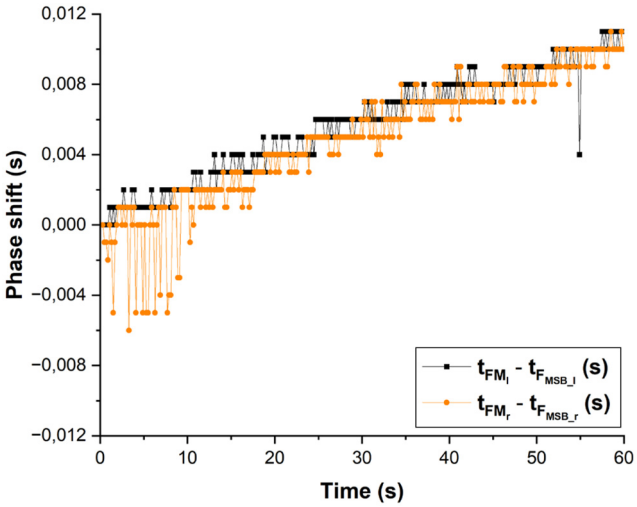

Source: Created by authors

signal noise. To mitigate the errors arising from the phase shift, both the calibration and measurement signals were divided into 1-s sections, resulting in a total of 60 sections, and each section was synchronized independently.

After synchronizing and splitting the signals into 1-s intervals, it is now possible to subtract the intervals FM_l, FM_r from either F_{MSB_l} or from F_{MSB_r}. Figure 6 illustrates these signals. Specifically, Figure 6(a) and 6(d) depict FM_l and FM_r, while 6(b) and 6(e) display FM_{MSB_l} and FM_{MSB_r}, respectively. The recalculated signals $FM_l - F_{MSB\_l}$ and $FM_r - F_{MSB\_r}$ are shown in 6(c) and 6(f).

After determining $FM_l - F_{MSB\_l}$ and $FM_r - F_{MSB\_r}$, $F_{dp-corr}$ is calculated according to formula (2). The resulting $F_{dp-corr}$ values, along with the corresponding normal force, are presented in Figure 7(a) and the COF is obtained according to formula (3), shown in Figure 7(b). Figure 7(b) illustrates 10 sections, each representing a stroke. For the analysis, we discard the incomplete data points in the first section, resulting in nine remaining sections for the 0 to 1 s interval. Subsequently, there are 10 strokes for each 1-s interval, except for the 59- to 60-s interval, where we again have nine sections. The data loss at the start and end of the data set is due to preceding synchronization calculations.

To estimate the uncertainty and the propagation of error, the decomposition of means and standard deviation method was followed (Altman *et al.*, 2013), which is described below. It is accepted that for this data a more sophisticated statistical analysis could better describe the error; however, across the current data sets, effects from controlled parameters can be observed and analysed.

In Figure 7(b), the asterisks denote the static friction values. To calculate the dynamic friction value for each section, we average

Figure 6 In (a) and (d), FM_l and FM_r are shown. In (b) and (e), F_{MSB_l} and F_{MSB_r} are displayed. The recalculated signals, $FM_l - F_{MSB\_l}$ and $FM_r - F_{MSB\_r}$, are shown in (c) and (f), respectively

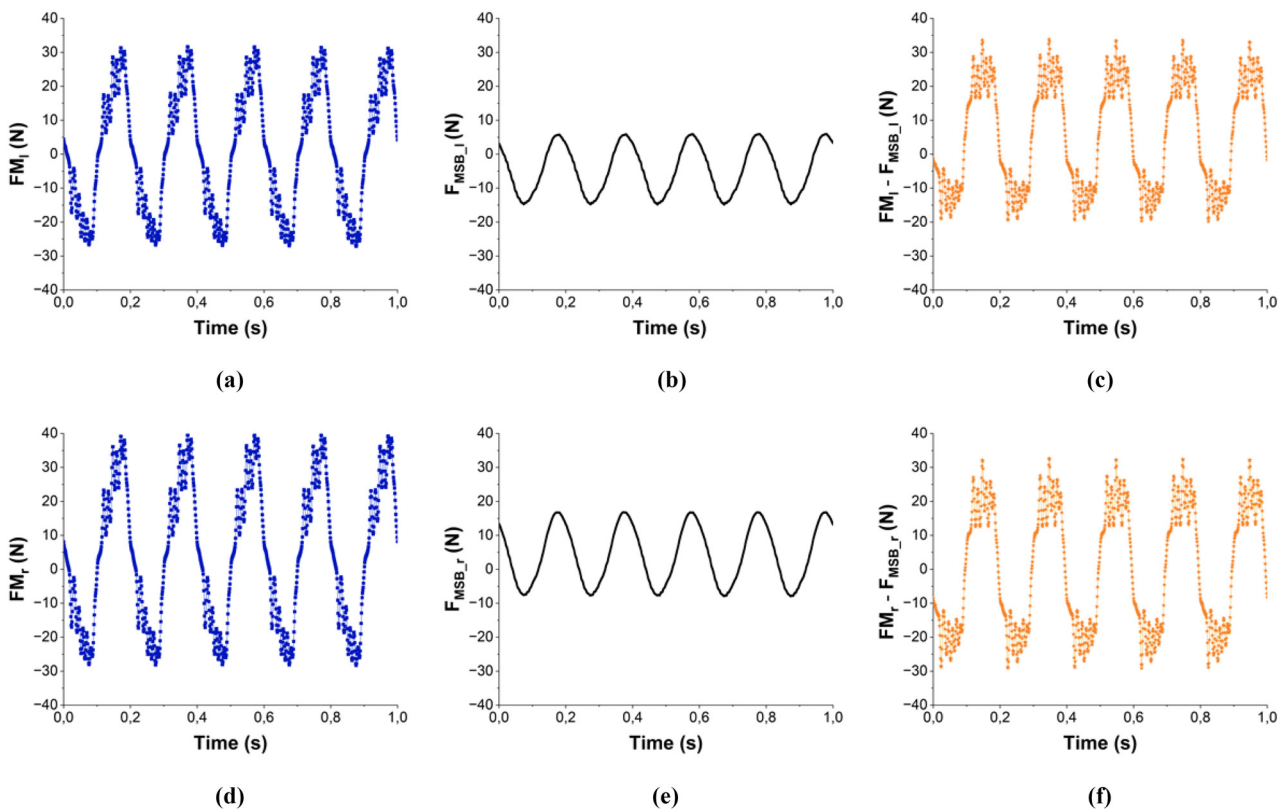

Source: Created by authors

Figure 7 (a) illustrates the $F_{dp-corr}$ values and their corresponding normal force. The coefficient of friction (COF) denoted by asterisks is obtained in (b). The start and endpoints for the calculation of the dynamic friction are marked with black diamonds within each section

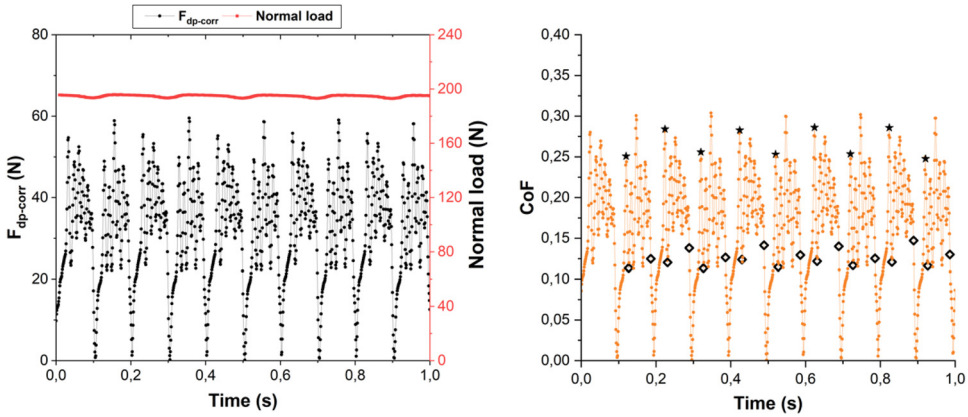

(a) (b)

Source: Created by authors

the values between the black diamonds within that section. By applying this method, we obtain nine values for the static friction coefficient and nine averaged values for the dynamic friction coefficient from the interval 0 to 1 s. These values are used to calculate the average static friction coefficient and averaged dynamic friction coefficient, along with their corresponding standard deviations.

Because there are multiple data points from which the average dynamic friction coefficient is derived and there are multiple cycles in a single experiment, the combined mean and standard deviation method is applied. Firstly, the average dynamic coefficient of friction, its standard deviation and variance are calculated for each semi-cycle (subgroup). Next, the statistics of each subgroup are combined to obtain the overall average and standard deviation for each second of the measurement.

3. Experimental

3.1 Materials and coatings

The base material of the upper specimen was aluminium Al6082 which was additionally plasma chemically oxidized (PCO, layer thickness 20 μm). The PCO layer was used as a support layer on which an anti-friction coating containing MoS_2/graphite/PTFE was applied (Rz 5 $\pm$ 1 μm). The lower disk polymer samples were made of polyketone (PK). During the production of the polymer samples, special care was taken to preserve the moulded skin as a tribological contact surface. The choice of materials and test conditions are based on a possible sealing system in a rotary compressor. PK is considered a suitable material for this application as it has good frictional and wear properties; however, it also has better dimensional stability under high loads in comparison to other sealing materials.

3.2 Tribological tests

The experiments were conducted at 90°C under 10 bar chamber pressure, with an oscillation frequency of 5 Hz and a stroke of 6 mm. The contact area averaged 52 mm^2, and the nominal contact pressure was 3.75 MPa. The tests were carried out under unlubricated sliding conditions.

The experiment was conducted in the following manner. Initially, calibration data was recorded for 60 s at a sampling rate of 1,000 Hz, with the samples not in contact. Then the samples were brought into contact, and a 60-s test was performed at the same sampling rate of 1,000 Hz. Afterwards, the sampling rate was reduced to 1 Hz, and a 120-min test was performed. The reason for reducing the sampling rate from 1,000 Hz to 1 Hz in the 120-min test was due to the limitations of the RVM measuring system, which is not designed to handle high sampling rates for extended durations exceeding 60 min. Finally, the sampling rate was set back to 1,000 Hz, and another 60-s test was carried out. With the measurement data recorded at a sampling rate of 1,000 Hz, the static and dynamic friction coefficients can be determined using the evaluation method described above.

4. Results and discussion

In Figure 8, the coefficient of friction results from two test series with the selected material pairing of PK and coated aluminium are presented. The shown data are processed with the algorithms explained in Section 2, and the mean values of static and dynamic friction with their standard deviation (grey shaded) are displayed.

For both test series, the static and dynamic coefficients of friction from the 60-s tests before and after the 120-min tests are presented on the left and the right side of the figure, respectively, while the average coefficient of friction (average values over 1 s) from the 120-min tests is presented in the middle of the figure. In the graphs with the static and the dynamic coefficients of friction, the average coefficient of friction (average values over 1 s) is presented for comparative purposes as well.

In Figure 8, the dynamic friction was always lower than the static, both before and after the 120-min test. Before the 120-min test, the static coefficient of friction was around 0.2 in the first test series, and in the second test series, it increased

Figure 8 Coefficient of friction from two test series with polyketone against coated aluminium

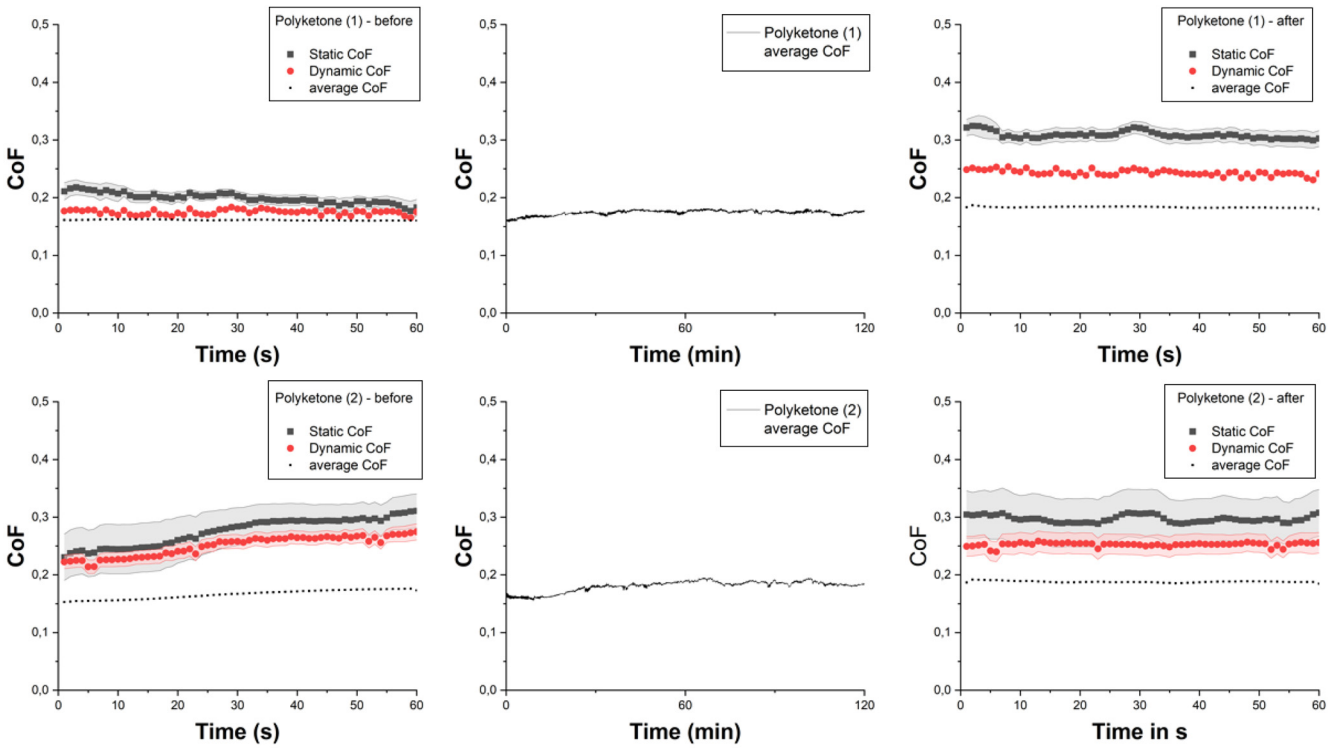

Notes: On the left and the right side of the figure, the static and the dynamic coefficients of friction from 60-s tests before and after the 120-min tests are presented, respectively, while the average coefficient of friction from the 120-min tests (average values over 1 s) is presented in the middle of the figure. For comparative purposes, in the graphs with the static and the dynamic coefficients of friction, the average coefficient of friction (average values over 1 s) with their standard deviation (grey shaded) presented as well
Source: Created by authors

from 0.2 to 0.3 during the 60 s of sliding. In both test series, the dynamic coefficient of friction followed the same trend as the static coefficient of friction while being approximately 10% lower before the 120-min test. After the 120-min test, the difference between the static and the dynamic coefficient of friction increased, which was primarily due to the increased static friction. After the 120-min test, in both test series, the static coefficient of friction had values of around 0.3, while the dynamic coefficient of friction was around 0.25, which is around 20% lower. This indicates that with the wear of the polymer sample under CO_2 atmosphere, adhesion between the polymer and the counter-body increases, which could in the long run lead to stick–slip effects.

It should be noted that the average coefficient of friction (average values over 1 s) is always lower than the dynamic coefficient of friction, which is counterintuitive as one would expect the average values should lie between the static and the dynamic ones. However, the average values are lower because they include the zero-values from the turning points as well (see Figure 7). The zero-values lower the average coefficient of friction as compared to the dynamic coefficient of friction where only the data points during sliding are considered.

During the 120-min test, the average coefficient of friction was stable at around 0.16 in both test series, and only a slight increase in friction was observed when comparing the values at the beginning and the end of the test. The difference is significantly lower as when comparing the static and dynamic friction values before and after the 120-min test. This shows the importance of evaluating the static and the dynamic coefficients of friction separately because the amount of information that is lost due to averaging is higher than one would expect.

5. Conclusions

In the present study, it was shown that:

- An experimental setup for testing tribological pairings under a gas atmosphere at pressures up to 10 bar was successfully developed and allows for testing under contact conditions that are close to real applications, such as compressors and expanders.
- A methodology for the evaluation of the coefficient of friction values separately from the spring forces is reliable and enables an in-depth insight into the static and dynamic friction of the tested material pairings.
- The values of the average coefficient of friction were lower than the static and the dynamic ones because in the average, all measured values over a time frame of 1 s are considered. This includes the zero-values from the turning points which lower the average as compared to the static and the dynamic coefficients of

friction where only the data points during sliding are considered.

- The difference between the static and the dynamic coefficients of friction increased after a 120-min sliding test, which indicates that with the sliding wear of the polymer sample under CO_2 atmosphere, adhesion between the polymer and the counter-body increases, which could in the long run lead to stick–slip effects.
- A separate evaluation of the static and the dynamic coefficient of friction is crucial for the in-depth understanding of the adhesion effects of the tested material pairings because the amount of information that is lost due to averaging the measured friction values is higher than one would expect.
- To the knowledge of the authors, this work provides the first method for interpreting, analysing and displaying data from a pressurised reciprocal tribometer, accounting for bellow behaviour.

5.1 Future work

- A detailed discussion of friction and wear mechanisms as well as stick–slip phenomena will be discussed in a further planned publication.

References

Altman, D., Machin, D., Bryant, T. and Gardner, M. (2013), *Statistics with Confidence: Confidence Intervals and Statistical Guidelines*, 2nd ed., Wiley, Hoboken.

Buckley, D.H. (1981), *Surface Effects in Adhesion, Friction, Wear, and Lubrication*, Elsevier, Amsterdam.

Dascalescu, D., Polychronopoulou, K. and Polycarpou, A.A. (2009), "The significance of tribochemistry on the performance of PTFE-based coatings in CO2 refrigerant environment", *Surface and Coatings Technology*, Vol. 204 No. 3, pp. 319-329, doi: 10.1016/j.surfcoat.2009.07.042.

Demas, N.G. and Polycarpou, A.A. (2008), "Tribological performance of PTFE-based coatings for air-conditioning compressors", *Surface and Coatings Technology*, Vol. 203 Nos 3/4, pp. 307-316, doi: 10.1016/j.surfcoat.2008.09.001.

Eggers, R. (2005), "Sorption und Schwellung von Polymeren in transkritischen CO_2-Kältekreisläufen", *DKV Berichte*, p. AA.II.1.

Kus, B. and Nekså, P. (2013), "Oil free turbo-compressors for CO_2 refrigeration applications", *International Journal of Refrigeration*, Vol. 36 No. 5, pp. 1576-1583, doi: 10.1016/j.ijrefrig.2013.03.002.

Ma, Y., Liu, Z. and Tian, H. (2013), "A review of transcritical carbon dioxide heat pump and refrigeration cycles", *Energy*, Vol. 55, pp. 156-172, doi: 10.1016/j.energy.2013.03.030.

Mishina, H. (1995), "Chemisorption of diatomic gas molecules and atmospheric characteristics in adhesive wear and friction of metals", *Wear*, Vol. 180 Nos 1/2, pp. 1-7, doi: 10.1016/0043-1648(95)80003-4.

Myshkin, N.K., Petrokovets, M.I. and Kovalev, A.V. (2005), "Tribology of polymers: adhesion, friction, wear, and mass-transfer", *Tribology International*, Vol. 38 Nos 11/12, pp. 910-921, doi: 10.1016/j.triboint.2005.07.016.

Nunez, E.E., Yeo, S.M. and Polycarpou, A.A. (2010), "Tribological behavior of PTFE, PEEK, and fluorocarbon-based polymeric coatings used in air-conditioning and refrigeration compressors", p. 9.

Teoh, Y.H., How, H.G., Le, T.D., Nguyen, H.T., Loo, D.L., Rashid, T. and Sher, F. (2023), "A review on production and implementation of hydrogen as a green fuel in internal combustion engines", *Fuel*, Vol. 333, p. 126525, doi: 10.1016/j.fuel.2022.126525.

Velkavrh, I., Ausserer, F., Klien, S., Voyer, J., Ristow, A., Brenner, J., Forêt, P. and Diem, A. (2016), "The influence of temperature on friction and wear of unlubricated steel/steel contacts in different gaseous atmospheres", *Tribology International*, Vol. 98, pp. 155-171, doi: 10.1016/j.triboint.2016.02.022.

Yeo, S.M. and Polycarpou, A.A. (2012), "Tribological performance of PTFE- and PEEK-based coatings under oil-less compressor conditions", *Wear*, Vol. 296 Nos 1/2, pp. 638-647, doi: 10.1016/j.wear.2012.07.024.

Corresponding author

Florian Ausserer can be contacted at: e1137832@student.tuwien.ac.at